Statistical Design of a 3D Microarray with Position-Encoded Microspheres

Pinaki Sarder and Arye Nehorai
Department of Electrical and Systems Engineering
Washington University in St. Louis
One Brookings Drive, St. Louis, MO 63130, USA
Email: {psarde1, nehorai}@ese.wustl.edu
Phone: 314-935-7520 Fax: 314-935-7500

***Abstract*—We propose a three-dimensional (3D) microarray device with fixed distance between the microspheres. The microspheres in the new device have controllable positions. To design the layout of our proposed device, we consider an optimal statistical performance analysis for imaging the microspheres. We compute the posterior Cramér-Rao bound on the error in estimating the unknown imaging parameters and use the bound to compute the minimal distance between the microspheres, which provides a desired level of statistical imaging performance. We illustrate our concept using a numerical example. The proposed microarray has high sensitivity, efficient packing density, and guaranteed imaging performance. It identifies targets based on the microspheres' locations, allowing significantly simplified imaging analysis.**

I. Introduction

Microarray devices are used to measure concentrations of targets such as mRNAs, proteins, antibodies, and cells. Applications include medical screening, drug discovery, and gene sequencing. Conventional microarrays used in clinical practices are primarily 2D.

Recently, a new 3D microarray technology has been developed [1], [2]. The main advantages of 3D microarrays over conventional 2D microarrays are their directional binding capability and higher sensitivity [1]. They consist of optically encoded microspheres for bio-targeting. Namely, the microspheres contain quantum-dot (QD) barcodes to identify the targets. Their surfaces are conjugated with molecular probes. Optical reporters (e.g., fluorescent dyes, QDs, nanospheres) are employed to quantify the target concentrations [1], [3]. Imaging is performed using a fluorescence microscope and a CCD detector.

In existing 3D microarrays, the microspheres are typically randomly placed on a substrate. Such random placement of the microspheres renders their packing inefficient. It also hampers the quality of the imaging in areas where the microspheres are closely clustered, and it makes the automatic imaging analysis difficult. Additionally, the existing 3D microarrays are prone to errors in identifying the targets, due to noise in the measured spectra from their QD barcodes.

In this paper, we propose a 3D microarray layout with determinate microsphere positions. These microspheres are thus position encoded to enable identifying the targets. We then propose a method of selecting the optimal positioning of the microspheres, using a parametric measurement model for the microsphere imaging and using statistical performance bounds on the error in estimating the unknown imaging parameters. The feasibility of implementing the proposed 3D microarray layout with the position-encoded microspheres is being demonstrated in a parallel research effort.

We first construct a statistical measurement model, assuming that the imaging is space-invariant and modeling the 3D point-spread function (PSF) using basis functions. The noise is considered to be additive Gaussian and the unknown model parameters to be random, with known prior distributions. We optimize the design by computing the posterior Cramér-Rao bound (PCRB) [4] on the error in estimating the unknown parameters. We define a performance measure, namely the trace of the PCRB [5] sub-matrix, for estimating the levels of the target concentrations as a function of the distance between the microspheres. We then compute the minimal distance between the microspheres that still provides a desired level of statistical performance in imaging.

We illustrate our concept of optimal microsphere positioning using a numerical example. Namely, we compute the optimal distance between the microspheres corresponding to the desired performance level. The result indicates that the minimal spacing between the neighboring microspheres' centers should be around 10 μm for imaging of target-less microspheres of radius 2.5 μm.

The paper is organized as follows. Section II describes the layout and imaging of the position-encoded microarray. Section III presents our proposed device design framework, and Section IV presents a corresponding numerical example. We conclude in Section V.

II. Position-Encoded Microarray Device

In this section, we discuss the configuration of the proposed microarray and its image-acquisition procedure.

A. Sensing Device Configuration

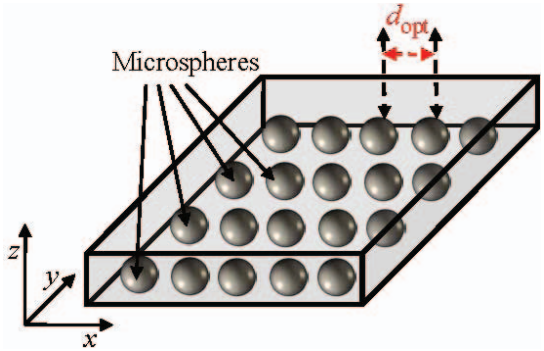

Fig. 1. Schematic diagram of a position-encoded three-dimensional microarray device that employs optimal separation.

Figure 1 illustrates a schematic diagram of a position-encoded 3D microarray device that we will optimally design by employing our proposed optimal separation between the microspheres ($\sim$5 μm in diameter). In this illustration, we assume that all the microsphere centers are positioned in a plane parallel to the xy plane. For simplicity, we represent the microspheres without their dedicated receptors. In our proposed device, the microspheres are polystyrene, and the receptors are antibody molecules.

978-1-4244-5180-7/09/$26.00 ©2009 IEEE

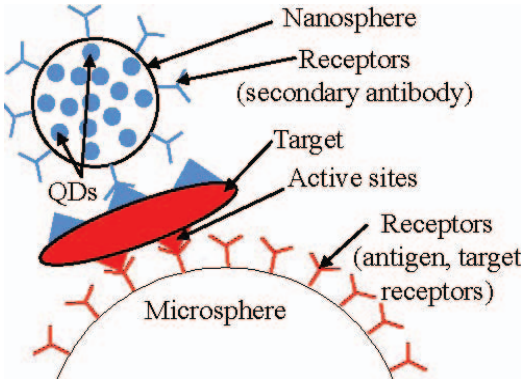

Fig. 2. A target molecule is captured on a microsphere.

To detect and quantify the targets, we use nanospheres (∼100 nm in diameter) embedded with identical QDs and conjugated with receptors. The nanospheres allow label-free targeting (targets do not contain any optical reporter, and thus their structures and chemical properties remain unchanged), on-off signaling, and enhance the detection sensitivity [1]. The targets are captured by the microspheres on one side, and they are tagged by the nanospheres on their other side, see Figure 2.

Thus, the main differences (mentioned so far) between the configurations of the proposed and existing 3D microarrays are the proposed position encoding and optimal selection of the minimal distance between the microspheres to estimate the target concentrations with a desired accuracy.

Some of the key advantages of our proposed device over the existing 3D microarrays will be efficient packing, high sensitivity, simplified imaging, and guaranteed accuracy of the target-concentration estimates. Our proposed microarray eliminates target-identification errors because of the known positions of the microspheres.

B. Preparing and Collecting Data

To prepare the data, we propose to follow the procedure in [1], except for identifying the targets. Namely, a microfluid stream with the targets is passed through the sensors and a cocktail of nanospheres is periodically released [1]. The targets bind to the intended microsphere surfaces on one side and to the nanospheres on the other side (Figure 2, showing one target and one nanosphere as an example) [1]. All nanosphere QDs emit light upon excitation by UV light, and produce a source of light in the form of a spherical shell around each microsphere. These shell-light signals quantify the target concentrations. We identify the targets using the known positions of the microspheres. This is in contrast to other approaches [1], where the targets are identified by employing QD barcodes in the microspheres, with possible errors.

To collect the data and obtain the images, we follow again the procedure in [1]. Namely, to image the target-captured specimen, a fluorescence microscope is focused at different depth planes of the ensemble, parallel to the xy plane of the target-free device shown in Figure 1. That produces a series of 2D cross-section images of the lights emitted by the nanosphere QDs [6]. Thus, each cross-section image of the spherical shell light formed around a microsphere forms the image of a ring. To capture the images, a CCD detector, with high sensitivity, i.e., with high quantum efficiency [7], is employed.

III. Statistical Design for Microsphere Placement

In this section, we present our proposed statistical method for computing the minimal distance between two neighboring microspheres. We first describe the measurement model for fluorescence microscopy imaging of our proposed device. After that we present the prior model of the unknown random parameters. We then derive the performance bounds on the estimation errors, for the statistical design.

A. Measurement Model

The measurement at the CCD detector output, in fluorescence microscopy imaging of a QD illuminating object, is (see [8])

$$g(x,y,z;\boldsymbol{\varphi}) = \tilde{s}(x,y,z;\boldsymbol{\varphi}) + w_{\mathrm{p}}(x,y,z;\boldsymbol{\varphi}) + w_{\mathrm{c}}(x,y,z), \quad (1)$$

where $x \in \{x_1, x_2, \ldots, x_K\}$, $y \in \{y_1, y_2, \ldots, y_L\}$, and $z \in \{z_1, z_2, \ldots, z_M\}$; $\boldsymbol{\varphi}$ is the unknown random parameter vector in imaging; $\tilde{s}(x,y,z;\boldsymbol{\varphi})$ is the microscope output; $w_{\mathrm{p}}(x,y,z;\boldsymbol{\varphi})$ is a zero-mean Gaussian noise with variance $\tilde{s}(\cdot)/\beta$, and β is the reciprocal of the photon-conversion factor [9]; $w_{\mathrm{p}}(x,y,z;\boldsymbol{\varphi})$ models the interference due to the photon counting process in the CCD detector, and is independent from voxel to voxel; $w_{\mathrm{c}}(x,y,z)$ models the background noise which is a zero-mean Gaussian noise with variance σ_{c}^2; $w_{\mathrm{c}}(x,y,z)$ is independently and identically distributed from voxel to voxel, and is statistically independent with $w_{\mathrm{p}}(x,y,z;\boldsymbol{\varphi})$. Thus, $g(x,y,z;\boldsymbol{\varphi})$ is Gaussian distributed with mean $\tilde{s}(\cdot)$ and variance $\tilde{s}(\cdot)/\beta + \sigma_{\mathrm{c}}^2$, independent from voxel to voxel [8]. In this paper, we assume β and σ_{c}^2 are known. They can be estimated from the images of target-free microspheres embedded with QDs.

Assuming a space-invariant microscopy, the microscope's output is given by (see, [6])

$$\tilde{s}(x,y,z;\boldsymbol{\varphi}) = s(x,y,z;\boldsymbol{\theta}) \otimes h(x,y,z;\boldsymbol{\tau}), \quad (2)$$

where $\boldsymbol{\varphi} = [\boldsymbol{\theta}^T, \boldsymbol{\tau}^T]^T$, $\boldsymbol{\theta}$ is the unknown random parameter vector of the QD illuminating object $s(x,y,z;\boldsymbol{\theta})$, $\boldsymbol{\tau}$ is the unknown random parameter vector of the microscope PSF $h(x,y,z;\boldsymbol{\tau})$, and $\otimes$ denotes the convolution operation.

We group the measurements into a vector form:

$$\boldsymbol{g} = \tilde{\boldsymbol{s}} + \boldsymbol{w}_{\mathrm{p}} + \boldsymbol{w}_{\mathrm{c}}, \quad (3)$$

where $\boldsymbol{g}$, $\tilde{\boldsymbol{s}}$, $\boldsymbol{w}_{\mathrm{p}}$, and $\boldsymbol{w}_{\mathrm{c}}$ are $(KLM \times 1)$–dimensional vectors whose $(KL((z-z_1)/\Delta z) + K((y-y_1)/\Delta y) + ((x-x_1)/\Delta x) + 1)^{\mathrm{th}}$ components are $g(\cdot)$, $\tilde{s}(\cdot)$, $w_{\mathrm{p}}(\cdot)$, and $w_{\mathrm{c}}(\cdot)$, respectively; $\Delta x = (x_{k+1} - x_k)$ ($\forall\ k = 1$ to $(K-1)$) and similarly for Δy and Δz.

Object Model (Nanosphere QD Intensity Profile of Two Neighboring Microspheres): We consider two neighboring microspheres, separated by a distance d, to model the object of interest for the design. In this object model, we assume that the target concentration is high, and/ or the time period of the sensing is sufficiently long. We thus assume that the microspheres are completely surrounded by their respective targets, the targets are surrounded in turn by attached nanospheres (Figure 2), and the object in our analysis is modeled by considering these nanospheres' QD lights. The lights from the nanosphere QDs of the target-captured microspheres produce shell-shaped objects, see Section II-B.

We model the object using two parametric neighboring shells at a separation distance d apart:

$$s(x,y,z;\boldsymbol{\theta}) = s_{\mathrm{sh}}(x,y,z;A_1) + s_{\mathrm{sh}}(x-d,y,z;A_2), \quad (4)$$

where $\boldsymbol{\theta} = [A_1, A_2]^T$ and A_1 and A_2 are the unknown random intensity levels, i.e., the target concentration levels, per voxel of the single shells $s_{\mathrm{sh}}(x,y,z;A_1)$ and $s_{\mathrm{sh}}(x-d,y,z;A_2)$, respectively. Here a

single shell, $s_{\rm sh}(\cdot)$, centered at the origin $\{x_{\rm c}, y_{\rm c}, z_{\rm c}\} = \{0,0,0\}$ of the Cartesian coordinates, is defined as follows:

$$s_{\rm sh}(x,y,z;A) = \begin{cases} A & \text{if } \ r_1 \le \sqrt{x^2+y^2+z^2} \le r_2, \\ 0 & \text{otherwise,} \end{cases} \tag{5}$$

where r_1 and r_2 are the known radii of the shell.

PSF Model: We consider the parametric widefield fluorescence microscope 3D Gaussian PSF model [8] to be

$$h(x,y,z;\boldsymbol{\tau}) = \exp\left(-\frac{x^2+y^2}{2\sigma_1^2} - \frac{z^2}{2\sigma_2^2}\right), \tag{6}$$

where $\boldsymbol{\tau} = [\sigma_1^2, \sigma_2^2]^T$. This model assumes that the Gaussian functions are centered at the origin of the PSF and they are separable along the xy-plane and the z-direction. The advantage of using this PSF model is that it preserves the symmetry and the asymmetry of the classical Gibbson and Lanni PSF model [10] along the focal planes and the optical direction, respectively.

B. Prior Models

Assume the prior distributions of the unknown parameters as

$$\sigma_i^2 \sim \mathcal{N}(\mu_{\tau i}, \sigma_{\tau i}^2), \qquad \{i = 1,2\}, \tag{7}$$

$$A_1, A_2 \sim \mathcal{N}(\mu_A, \sigma_A^2), \tag{8}$$

where $\mathcal{N}(\alpha, \delta^2)$ denotes a Gaussian random variable with mean α and variance δ^2 [11], and $\mu_{\tau i}, \sigma_{\tau i}^2$ $(i = 1,2)$, μ_A, and σ_A^2 are the known prior parameters. We assume that the prior distributions of the unknown parameters are statistically independent of each other. Note that σ_i^2 and A_i $(i = 1,2)$ are positive, and hence truncated normal distributions would be more appropriate prior choices for them. In this paper, we assume that these parameters are sufficiently larger than zero, and hence the likelihood of obtaining their negative values is negligible using our current prior choice.

C. Performance Analysis

We compute the PCRB on the error in estimating the unknown parameters of (1) to optimize the design. After briefly presenting the concept of the PCRB, we introduce the joint likelihood of the measurement and the unknown parameters, and present the expressions of the elements of the (Fisher) information matrix. We then summarize our analytic strategy for computing the minimal distance between a pair of microspheres in our proposed microarray.

1) PCRB: Let $\boldsymbol{g}$ represents a vector of the measured data, $\boldsymbol{\varphi} = [\varphi_1, \varphi_2, \cdots, \varphi_n]^T$ be an n dimensional unknown random parameter to be estimated, $p_{G,\Phi}(\boldsymbol{g}, \boldsymbol{\varphi})$ be the joint probability density of the pair $(\boldsymbol{g}, \boldsymbol{\varphi})$, and $\boldsymbol{q}(\boldsymbol{g})$ is an estimate of $\boldsymbol{\varphi}$, which is a function of $\boldsymbol{g}$. The PCRB on the estimation error has the form

$$\boldsymbol{Q} = \mathrm{E}\Big[[\boldsymbol{q}(\boldsymbol{g}) - \boldsymbol{\varphi}][\boldsymbol{q}(\boldsymbol{g}) - \boldsymbol{\varphi}]^T\Big] \ge \boldsymbol{J}^{-1}, \tag{9}$$

where $\mathrm{E}(\cdot)$ denotes the statistical expectation with respect to the joint probability density function (pdf) $p_{G,\Phi}(\boldsymbol{g}, \boldsymbol{\varphi})$ and $\boldsymbol{J}$ is the $n \times n$ (Fisher) information matrix with the elements

$$J_{ij} = \mathrm{E}\left[-\frac{\partial^2 \log p_{G,\Phi}(\boldsymbol{g}, \boldsymbol{\varphi})}{\partial\varphi_i \partial\varphi_j}\right], \qquad i,j = 1,\ldots,n, \tag{10}$$

provided that the derivatives $\left(\frac{\partial^2(\cdot)}{\partial\varphi_i\partial\varphi_j}\right)$ and $\mathrm{E}(\cdot)$ in (9) and (10) exist. The inequality in (9) means that the difference $\boldsymbol{Q} - \boldsymbol{J}^{-1}$ is a positive semidefinite matrix. We compute the PCRBs on the errors in estimating the unknown random parameters in $\boldsymbol{\varphi}$ corresponding to the diagonal elements of the matrix $\boldsymbol{J}^{-1}$ [4], [12].

2) Likelihood Function: The joint log-likelihood function of the measurement $\boldsymbol{g}$ and the unknown random parameters $\boldsymbol{\varphi}$ using (1) is

$$\begin{aligned} \log p_{G,\Phi}(\boldsymbol{g}, \boldsymbol{\varphi}) \approx & \\ & -\sum_x \sum_y \sum_z \left[\frac{\big(g(\cdot) - \tilde{s}(\cdot)\big)^2}{2\big(\frac{\tilde{s}(\cdot)}{\beta} + \sigma_{\rm c}^2\big)} + \frac{1}{2}\log\left(\frac{\tilde{s}(\cdot)}{\beta} + \sigma_{\rm c}^2\right)\right] \\ & -KLM \sum_{i=1}^{2}\left[\frac{(A_i - \mu_A)^2}{2\sigma_A^2} + \frac{(\sigma_i^2 - \mu_{\tau i})^2}{2\sigma_{\tau i}^2}\right]. \end{aligned} \tag{11}$$

3) Information Matrix: We derive the elements of the (Fisher) information matrix $\boldsymbol{J}$ using (10) for computing the PCRBs on the error in estimating the unknown random parameters in $\boldsymbol{\varphi} = [\varphi_1 = A_1, \varphi_2 = A_2, \varphi_3 = \sigma_1^2, \varphi_4 = \sigma_2^2]^T$, see Section III-C1. We have

$$\frac{\partial s(\cdot)}{\partial A_1} = \begin{cases} 1 & \text{if } \ r_1 \le \sqrt{x^2+y^2+z^2} \le r_2, \\ 0 & \text{otherwise;} \end{cases} \tag{12}$$

$$\frac{\partial s(\cdot)}{\partial A_2} = \begin{cases} 1 & \text{if } \ r_1 \le \sqrt{(x-d)^2+y^2+z^2} \le r_2, \\ 0 & \text{otherwise;} \end{cases} \tag{13}$$

$$\frac{\partial h(\cdot)}{\partial \sigma_1^2} = \frac{(x+y)^2}{2\sigma_1^4}\exp\left(-\frac{x^2+y^2}{2\sigma_1^2} - \frac{z^2}{2\sigma_2^2}\right); \tag{14}$$

and

$$\frac{\partial h(\cdot)}{\partial \sigma_2^2} = \frac{z^2}{2\sigma_2^4}\exp\left(-\frac{x^2+y^2}{2\sigma_1^2} - \frac{z^2}{2\sigma_2^2}\right). \tag{15}$$

The expressions of the elements of the symmetric matrix $\boldsymbol{J}$ are

$$J_{ij} = \begin{cases} \frac{KLM}{\sigma_A^2} + \mathrm{E}_{\boldsymbol{\varphi}}\left[\sum_x \sum_y \sum_z \left(\frac{\partial s(\cdot)}{\partial\varphi_i} \otimes h(\cdot)\right)^2 o(\cdot)\right], \\ \qquad\qquad i = j \in \{1,2\}; \\ \frac{KLM}{\sigma_{\varphi_i}^2} + \mathrm{E}_{\boldsymbol{\varphi}}\left[\sum_x \sum_y \sum_z \left(s(\cdot) \otimes \frac{\partial h(\cdot)}{\partial\varphi_i}\right)^2 o(\cdot)\right], \\ \qquad\qquad i = j \in \{3,4\}; \\ \mathrm{E}_{\boldsymbol{\varphi}}\left[\sum_x \sum_y \sum_z \left(\frac{\partial s(\cdot)}{\partial\varphi_i} \otimes h(\cdot)\right)\left(\frac{\partial s(\cdot)}{\partial\varphi_j} \otimes h(\cdot)\right) o(\cdot)\right], \\ \qquad\qquad i = 1,\ j = 2; \\ \mathrm{E}_{\boldsymbol{\varphi}}\left[\sum_x \sum_y \sum_z \left(\frac{\partial s(\cdot)}{\partial\varphi_i} \otimes h(\cdot)\right)\left(s(\cdot) \otimes \frac{\partial h(\cdot)}{\partial\varphi_j}\right) o(\cdot)\right], \\ \qquad\qquad i \in \{1,2\},\ j \in \{3,4\}; \\ \mathrm{E}_{\boldsymbol{\varphi}}\left[\sum_x \sum_y \sum_z \left(s(\cdot) \otimes \frac{\partial h(\cdot)}{\partial\varphi_i}\right)\left(s(\cdot) \otimes \frac{\partial h(\cdot)}{\partial\varphi_j}\right) o(\cdot)\right], \\ \qquad\qquad i = 3,\ j = 4; \end{cases} \tag{16}$$

where $o(\cdot)$ is given by

$$o(x,y,z;\boldsymbol{\varphi}) = \tilde{s}(x,y,z;\boldsymbol{\varphi})(1 + 4\sigma_{\rm c}^2\beta^2) + \sigma_{\rm c}^2\beta(1 + 2\sigma_{\rm c}^2\beta^2). \tag{17}$$

We compute $\mathrm{E}_{\boldsymbol{\varphi}}[\cdot]$ in (16) with respect to the pdf

$$\begin{aligned} p_{\Phi}(\boldsymbol{\varphi}) = & \frac{1}{(2\pi\sigma_A\sigma_{\tau 1}\sigma_{\tau 2})^2} \\ & \times \exp\left[-\sum_{i=1}^{2}\left\{\frac{(A_i - \mu_A)^2}{2\sigma_A^2} + \frac{(\sigma_i^2 - \mu_{\tau i})^2}{2\sigma_{\tau i}^2}\right\}\right] \end{aligned} \tag{18}$$

using the Monte-Carlo integration estimation technique [13].

4) Computing the Minimal Distance: We define the performance measure as the sum of the PCRBs on the errors in estimating the target concentrations, i.e., as $(\mathrm{PCRB}(A_1) + \mathrm{PCRB}(A_2))$. We compute the optimal distance $d_{\rm opt}$ by analyzing the performance measure as a function of the distance d between the microspheres, to obtain a desired error in estimating the target concentrations.

IV. Numerical Example

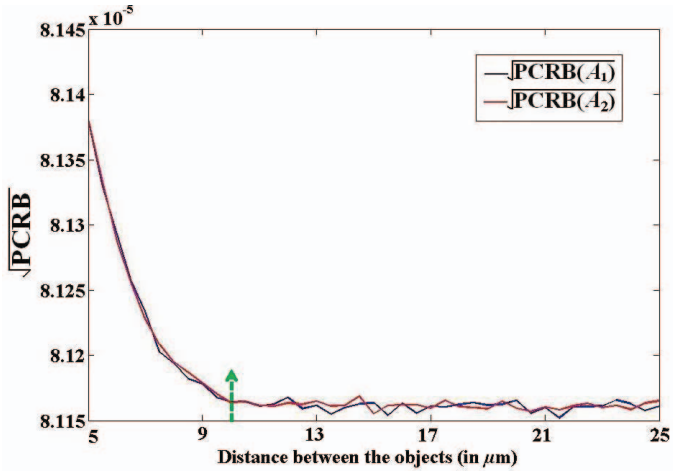

Fig. 3. Square root of PCRBs on the errors in estimating A_1 and A_2. The resulting optimal minimal spacing between target-free microspheres with diameter of 5 μm is 10 μm.

We illustrate our proposed concept for statistical design using a simple numerical example. We compute here the minimal distance for measuring the QD lights from a pair of neighboring target-free microspheres embedded with QDs [8], [14]. Particularly, we consider a spherical object model in (1), that we form using (5) by defining $r_1 = 0$ and $r_2 = 2.5$ μm. We also use realistic values of the design parameters (the prior parameters, the CCD parameter, and the background noise variance parameter). Namely, we use $\mu_A = 0.0053$, $\sigma_A^2 = 2.7589 \times 10^{-6}$, $\mu_{\tau 1} = 3.63$ $\mu\mathrm{m}^2$, $\sigma_{\tau 1}^2 = 0.02$ $\mu\mathrm{m}^4$, $\mu_{\tau 2} = 2.02 \times 10^{-3}$ mm^2, $\sigma_{\tau 2}^2 = 6.14 \times 10^{-8}$ mm^4, $\beta = 305$, $\sigma_{\mathrm{c}}^2 = 4.23 \times 10^{-6}$.

To obtain the values of the design parameters, we imaged multiple target-free microspheres embedded with QDs, each of which produces spherical-light signal with uniform intensity level [8]. Using the noise only section of the measured image, we first compute the background noise variance σ_{c}^2. We then estimate the sphere-intensity level and the PSF parameters from each microsphere image using our proposed maximum-likelihood method, see [8]. We compute the prior parameters, i.e., $\mu_{\tau i}, \sigma_{\tau i}^2$ $(i = 1, 2)$, μ_A, and σ_A^2, using the histograms of these estimates. We compute the CCD parameter β using the method-of-moments solution in [15].

In Figure 3, we show the square root of the PCRBs on the errors in estimating the intensity levels A_1 and A_2 as a function of distance between the object centers. Observe that when increasing the distance between the microspheres, the PCRBs first decrease, and then essentially flatten. In this case, we propose using the distance for which the PCRBs start leveling off as the optimal distance d_{opt} between the microspheres. In the current example, we find $d_{\mathrm{opt}} = 10$ μm by inspection (the green arrow in Figure 3), for the microspheres.

Observe that the curves in Figure 3 are similar, as we use the same prior distribution to define the QD intensity levels of the neighboring microspheres. In principle, we could use different prior distributions. In that case, the related PCRB values would be different. However, their corresponding curves would have a similar shape as the curves in Figure 3.

V. Conclusion

We have proposed an optimal design for positioning microspheres in microarrays, based on statistical performance analysis. Potential applications of our proposed position-encoded microarray include studies relating to molecular recognition, specificity of targeting molecules, protein-protein dimerization, high throughput screening assays for enzyme inhibitors, drug discovery, gene sequencing, etc.

In our future work, we will develop a statistical framework to automatically select the minimal distance between the microspheres, in analyzing the performance measure as a function of the distance between the microspheres. We are also implementing with our collaborators the position-encoded 3D microarray device using the minimal separation distance between the microspheres.

Acknowledgment

The authors thank Mr. Patricio S. La Rosa for his helpful comments.

References

[1] A. Mathur, *Image Analysis of Ultra-High Density, Multiplexed, Microsphere-Based Assays,* Ph.D. thesis, Northwestern University, IL., 2006.

[2] W. Xu, K. Sur, H. Zeng, A. Feinerman, D. Kelso, and J. B. Ketterson, "A microfluidic approach to assembling ordered microsphere arrays," *J. of Micromechanics and Microengineering,* vol. 18, pp. 075027, 2008.

[3] M. Han, X. Gao, J. Z. Su, and S. Nie, "Quantum-dot-tagged microbeads for multiplexed optical coding of biomolecules," *Nat. Biotechnol.,* vol. 19, pp. 631-635, 2001.

[4] H. L. van Trees, *Detection, Estimation and Modulation Theory,* New York: Wiley, 1968.

[5] K. Shah and B. Sinha, *Theory of Optimal designs,* New York: Springer-Verlag, 1989.

[6] P. Sarder and A. Nehorai, "Deconvolution methods of 3D fluorescence microscopy images: An overview," *IEEE Signal Proc. Magazine,* vol. 23, pp. 32-45, 2006.

[7] M. Christenson, "The application of scientific grade CCD cameras to biological imaging," *Imaging Neurons: A Laboratory Manual,* Ch. 6, R. Yuste, F. Lanni, A. Konnerth, Eds., pp. 23-32, 2000.

[8] P. Sarder and A. Nehorai, "Estimating locations of quantum-dot–encoded microparticles from ultra-high density 3D microarrays," *IEEE Trans. on NanoBioscience*, vol. 7, no. 4, pp. 284-297, Dec. 2008.

[9] D. L. Snyder and M. I. Miller, *Random Point Processes in Time and Space, Second Edition*, New York: Springer-Verlag, 1991.

[10] S. F. Gibson and F. Lanni, "Experimental test of an analytical model of aberration in an oil-immersion objective lens used in three-dimensional light microscopy," *J. Opt. Soc. Am. A.,* vol. 8, no. 10, pp. 1601-1612, 1991.

[11] A. Papoulis and S. U. Pillai, *Probability, Random Variables and Stochastic Processes, Fourth Edition*, McGraw-Hill Science, 2001.

[12] P. Tichavsky, C. H. Muravchik, and A. Nehorai, "Posterior Cramér-Rao bounds for discrete-time nonlinear filtering," *IEEE Trans. on Signal Processing,* vol. SP-46, pp. 1386-1396, 1998.

[13] G. Casella, *Monte Carlo Statistical Methods, Second Edition,* Springer Verlag, 2004.

[14] *http://www.crystalplex.com*

[15] F. Aguet, D. V. D. Ville, and M. Unser, "A maximum-likelihood formalism for sub-resolution axial localization of fluorescent nanoparticles," *Opt. Exp.*, vol. 13, pp. 10503-10522, 2005.